AFRL-RY-HS-TR-2011-0005

The Origin of the Log Law Region for Wall-bounded Turbulent Boundary Layer Flows

David W. Weyburne

AFRL/RYHC
80 Scott Drive
Hanscom AFB, MA 01731-2909

25 February 2011

Technical Report

APPROVED FOR PUBLIC RELEASE; DISTRIBUTION UNLIMITED

AIR FORCE RESEARCH LABORATORY
Sensors Directorate
Electromagnetics Technology Division
Hanscom AFB MA 01731-2909

NOTICE AND SIGNATURE PAGE

Using Government drawings, specifications, or other data included in this document for any purpose other than Government procurement does not in any way obligate the U.S. Government. The fact that the Government formulated or supplied the drawings, specifications, or other data does not license the holder or any other person or corporation; or convey any rights or permission to manufacture, use, or sell any patented invention that may relate to them.

This report was cleared for public release by the Electronic Systems Center Public Affairs Office for the Air Force Research Laboratory Electromagnetic Technology Division and is available to the general public, including foreign nationals. Copies may be obtained from the Defense Technical Information Center (DTIC) (http://www.dtic.mil).

AFRL-RY-HS-TR-2011-0005 HAS BEEN REVIEWED AND IS APPROVED FOR PUBLICATION IN ACCORDANCE WITH ASSIGNED DISTRIBUTION STATEMENT.

David W. Weyburne

DAVID W. WEYBURNE
Contract Monitor

DAVID F. BLISS, Acting Chief
Optoelectronic Technology Branch

Robert V. McGahan

ROBERT V. McGAHAN
Technical Communications Advisor
Electromagnetic Technology Division

This report is published in the interest of scientific and technical information exchange, and its publication does not constitute the Government's approval or disapproval of its ideas or findings.

REPORT DOCUMENTATION PAGE

Form Approved
OMB No. 0704-0188

Public reporting burden for this collection of information is estimated to average 1 hour per response, including the time for reviewing instructions, searching existing data sources, gathering and maintaining the data needed, and completing and reviewing this collection of information. Send comments regarding this burden estimate or any other aspect of this collection of information, including suggestions for reducing this burden to Department of Defense, Washington Headquarters Services, Directorate for Information Operations and Reports (0704-0188), 1215 Jefferson Davis Highway, Suite 1204, Arlington, VA 22202-4302. Respondents should be aware that notwithstanding any other provision of law, no person shall be subject to any penalty for failing to comply with a collection of information if it does not display a currently valid OMB control number. **PLEASE DO NOT RETURN YOUR FORM TO THE ABOVE ADDRESS.**

1. REPORT DATE *(DD-MM-YYYY)* 25 February 2011	**2. REPORT TYPE** Technical Report	**3. DATES COVERED *(From - To)*** 1 Jun 2010 – 8 Oct 2010
4. TITLE AND SUBTITLE The Origin of the Log Law Region for Wall-bounded Turbulent Boundary Layer Flows		**5a. CONTRACT NUMBER** IN-HOUSE **5b. GRANT NUMBER** **5c. PROGRAM ELEMENT NUMBER** 62204F
6. AUTHOR(S) David W. Weyburne		**5d. PROJECT NUMBER** 4916 **5e. TASK NUMBER** HC **5f. WORK UNIT NUMBER** 10
7. PERFORMING ORGANIZATION NAME(S) AND ADDRESS(ES) AFRL/RYHC 80 Scott Drive Hanscom AFB, MA 01731-2909 Source Code: 437890		**8. PERFORMING ORGANIZATION REPORT NUMBER**
9. SPONSORING / MONITORING AGENCY NAME(S) AND ADDRESS(ES) Electromagnetics Technology Division Sensors Directorate Air Force Research Laboratory 80 Scott Drive Hanscom AFB, MA 01731-2909		**10. SPONSOR/MONITOR'S ACRONYM(S)** AFRL/RYHC **11. SPONSOR/MONITOR'S REPORT NUMBER(S)** AFRL-RY-HS-TR-2011-0005

12. DISTRIBUTION / AVAILABILITY STATEMENT

DISTRIBUTION A: APPROVED FOR PUBLIC RELEASE: DISTRIBUTION UNLIMITED

13. SUPPLEMENTARY NOTES

The U.S. Government is joint author of this work and has the right to use, modify, reproduce, release, perform, display, or disclose the work. Cleared for Public Release by 66ABW-2011-0109, 7 February 2011.

14. ABSTRACT

The origin of the Log Law behavior of a wall-bounded turbulent boundary layer is outlined. The new theory of the origin of the Log Law starts with previous experimental observations that show that the turbulent boundary layer fluid undergoes rapid changes in the wall shear stress at any point on the wall. The main insight provided herein is that this rapid change in the wall shear stress corresponds to a rapid, quantifiable change in the location of the viscous sublayer toward and away from the wall in the velocity boundary layer. When this viscous layer is then spatially averaged, we theorize that the normal exponential-like decay of the viscous shear is stretched out in the tail region. The next step is to use various experimental results from the literature to show that the viscous sublayer, which is directly proportional to the second derivative of the velocity profile, extends much deeper into the boundary layer than previously thought. In fact it is shown that the viscosity effects extend all the way into the Log Law region where the spatially-averaged tail region begins to show a one-over-distance-from-the-wall-squared behavior. Hence, when the spatially-averaged second derivative profile is twice integrated to obtain the velocity profile perpendicular to the wall, one obtains the classic logarithmic profile behavior of the Log Law region of the turbulent boundary layer.

15. SUBJECT TERMS

Fluid Boundary Layers, Turbulent Flow, Log Law, Wall Shear Stress, Mean Viscous Location

16. SECURITY CLASSIFICATION OF:			**17. LIMITATION OF ABSTRACT**	**18. NUMBER OF PAGES**	**19a. NAME OF RESPONSIBLE PERSON**
a. REPORT	**b. ABSTRACT**	**c. THIS PAGE**			David W. Weyburne
Unclassified	Unclassified	Unclassified	SAR	29	**19b. TELEPHONE NUMBER** n/a

Standard Form 298 (Rev. 8-98)
Prescribed by ANSI Std. Z39.18

Table of Contents

List of Figures iv

Acknowledgments v

Summary 1

1. Introduction 2

2. Viscous Layer Description 3

3. The Log Law Revealed 6

4. Instantaneous Second Derivative Profile Model 6

5. Discussion 11

6. Conclusion 14

References 14

Appendix 1 17

Appendix 2 22

List of Figures

Figure 1. The solid line is the second derivative of the velocity of the Blasius [12] solution for laminar flow. 4

Figure 2. Diagrammatic depiction of flow along a wall undergoing separation. 5

Figure 3. The solid lines are the McKeon, *et. al*. [13] Super Pipe profiles plotted in plus units. The dashed line is the Log Law line. 7

Figure 4. The solid lines are the DeGraaff and Eaton [14] ZPG profiles plotted in plus units. The dashed line is the Log Law line. 7

Figure 5. The solid lines are the Österlund [15] SW981129 dataset plotted in plus units. The dashed line is the Log Law line. 8

Figure 6. The solid lines are the Zanoun and Durst [16] channel flow profiles plotted in plus units. The dashed line is the Log Law line. 8

Figure 7. Second derivative profiles of Wu and Moin [9] data plotted in plus units. 9

Figure 8. Same as Fig. 7 but with modified laminar profile such that c_f is 5 times larger. 10

Figure 9. Same as Fig. 7 but with modified laminar profile such that c_f =0.0005. 10

Figure 10. A recreation of Figure 7 from Obi, *et. al*. [8] showing a PDF of the instantaneous wall shear stress. 11

Acknowledgement

The author would like to thank the following groups and individuals for supplying their experimental datasets for inclusion in this manuscript: David DeGraaff and John Eaton; George Khujadze and Martin Oberlack; Jens Österlund; P. Roach and D. Brierly; Xiaohua Wu and Parviz Moin; Javier Jimenez and Sergio Hoyas; Beverley McKeon, J. Li, W. Jiang, J. Morrison, and Alexander Smits; El-Sayed Zanoun and Franz Durst; P. Schlatter, R. Örlü, Q. Li, G. Brethouwer, J. Fransson, A. Johansson, P. Alfredsson, and D. Henningson; S. Hoyas and J. Jimenez; Mark Simens, Javier Jiménez, Sergio Hoyas, Yoshinori Mizuno; W. Bauer; and K. Wieghardt and W. Tillmann.

Summary

The origin of the Log Law behavior of a wall-bounded turbulent boundary layer is outlined. The new theory of the origin of the Log Law starts with previous experimental observations that show that the turbulent boundary layer fluid undergoes rapid changes in the wall shear stress at any point on the wall. The main insight provided herein is that this rapid change in the wall shear stress corresponds to a rapid, quantifiable change in the location of the viscous sublayer toward and away from the wall in the velocity boundary layer. When this viscous layer is then spatially averaged, we theorize that the normal exponential-like decay of the viscous shear is stretched out in the tail region. The next step is to use various experimental results from the literature to show that the viscous sublayer, which is directly proportional to the second derivative of the velocity profile, extends much deeper into the boundary layer than previously thought. In fact it is shown that the viscosity effects extend all the way into the Log Law region where the spatially-averaged tail region begins to show a one-over-distance-from-the-wall-squared behavior. Hence, when the spatially-averaged second derivative profile is twice integrated to obtain the velocity profile perpendicular to the wall, one obtains the classic logarithmic profile behavior of the Log Law region of the turbulent boundary layer.

1. Introduction

Beginning with the pioneering work of Reynolds [1], there has been a concerted effort to find coordinate scaling parameters that make the scaled velocity profiles and shear-stress profiles taken at different stations along the flow appear to be nearly identical. For turbulent boundary layers, this search for "similarity" was mostly unsuccessful. This led to the practice of trying to find similarity in subregions of the whole profile. Perhaps the most successful case of partial similarity was developed by von Kármán [2] and Prandtl [3] and is known as the Logarithmic Law or "Log Law." The Log Law states that in a certain subregion of the turbulent boundary layer the average velocity in the streamwise x-direction $u(x, y)$ of a wall-bounded turbulent flow is given by

$$\frac{u(x,y)}{u} = \frac{1}{} \ln\left(\frac{yu}{}\right) + B \quad , \tag{1}$$

where y is the height perpendicular to the solid surface , is kinematic viscosity, and B are constants, and u is the Prandtl velocity scaling parameter, the so-called friction velocity.

The Log Law is widely believed to describe most, if not all, turbulent wall-bounded flows. Furthermore, many believe that the empirical constants, the so-called von Kármán constant, , and the additive constant, B, are universal. However, there seems to be little consensus about what these universal values actually are and whether the pipe flow constants are the same as the constants for flow over a plate. In addition, there does not seem to be any consensus as to the extent of the Log Law, *i.e.* which portion of the profile is actually described by the Log Law.

The theoretical work on the Log Law has been unable to answer any of these critical questions. The theoretical work on the Log Law began with von Karman [2] and Prandtl [3] who postulated that the Log Law could be derived from a simple eddy viscosity/mixing length argument. An alternative derivation of the Log Law was made by Millikan [4] using a inner-outer layer matching argument. However, none of the available derivations, including those using dimensional arguments or the Lie-group analysis of Oberlack [5], provide any insight into the physical processes in a turbulent boundary layer that create the logarithmic velocity profile. Therefore, it is evident that a physical model of the turbulent boundary layer that would explain the origin of the Log Law is lacking. George [6] has pointed out that even though there does not seem to be a solid theoretical foundation for the Log Law for flow over-a-plate boundary layers, there is ample empirical evidence that supports its existence.

In what follows, we outline a new theory to explain the existence of the Log Law region of a wall-bounded turbulent boundary flow. The key insight comes from the fact that experimental work [7-9] makes it clear that the wall shear stress $_w$, or equivalently, the skin friction coefficient c_f, undergo very large fluctuations at any point on the wall in the turbulent flow region. The most important contribution provided herein is that these large changes in the wall shear stress induce quantifiable fluctuations in the location of the viscous sublayer in the boundary layer. The quantification will be detailed in the next section where it will be shown that the fluctuations of the wall shear stress causes the second derivative profile, which defines the viscous sublayer, to move closer or further away from the wall, depending the on the instantaneous wall shear stress value.

The question then becomes is how this fluctuation of the viscous sublayer affects the Log Law region of the fluid. Conventional thinking is that the viscous sublayer only extends from the wall

to about $y^+ \cong 30$ into the fluid [6]. This would seem to make any fluctuations in the location of viscous sublayer irrelevant to the Log Law which is generally assumed to just start at $y^+ \cong 30$ and extend much deeper into the fluid [6]. Resolution to the conundrum comes from the use of experimental results to show that the viscous shear layer actually extends much deeper into the boundary layer than previously thought. In fact it extends all the way into the Log Law region. To show this, we take various experimental velocity profile datasets available in the literature and numerically differentiate the data twice. What we find is that the second derivative profiles in the Log Law region are many orders of magnitude down from the peak value. Never-the-less, we find that in the Log Law region, the second derivative profiles do track the second derivative of Eq. 1 very well. Therefore fluctuations in the second derivative profile will have a direct effect on the Log Law region of the fluid.

These two insights are well supported by experimental evidence and form the basis of the new theory. That is, time fluctuations of the wall shear stress cause a spatial fluctuation of the second derivative profile towards-away from the wall and these spatial fluctuations reach all the way into the Log Law region of the boundary layer. The major unknown at this point is that the shape of the instantaneous second derivative is not known nor is it easily experimentally accessible in a wind tunnel. Alternatively one could use DNS computer results. While this is an option we are presently exploring, it was not deemed possible from a time perspective for inclusion in this manuscript. This is where our conjecture comes into play. We theorize that the tail region of the turbulent boundary layers instantaneous viscous sublayer has the same tail behavior as the laminar flow case. What we actually expect to see is a distorted laminar-like second derivative profile tail. However, for illustrative purposes we will assume the entire shape is laminar-like. For wall-bounded laminar flow, it is known that for the laminar flow case the second derivative profile decays in a Gaussian-like manner [10]. What we think happens in the turbulent case is that as one does the time average of the spatially fluctuating second derivative profile, the Gaussian-like decay of the instantaneous second derivative profile is stretched out into a one-over-distance-from-the-wall-squared behavior, at least in the Log Law region on the boundary layer. The fact that the viscous sublayer extend all the way into the Log Law region means that when the second derivative profile is twice integrated to obtain the velocity profile perpendicular to the wall, one obtains the classic logarithmic profile of the Log Law.

The simplified model starts by assuming that the entire instantaneous second derivative profile has roughly the same shape as the laminar flow shear profile. We then present second derivative velocity profiles plots that show what would happen if the wall shear stress of a laminar-like profile is changed to a value corresponding to the maximum and minimum measured instantaneous shear stress values. Experimental results indicate that the turbulent boundary layer at any point on the wall is fluctuating between these maximum and minimum values. Hence one would expect that given the frequency of occurrence, one could do a spacial average to show how the normal Gaussian type decay of the velocity shear profile is changed into a one-over-distance-from-the-wall-squared behavior.

To begin, we first work out the relationship between the wall shear stress fluctuations and the location of the viscous shear layer of the boundary layer.

2. Viscous Layer Description

For the work herein, it is important to understand the relationship between the wall shear stress and the location of the viscous layer of the wall-bounded turbulent boundary layer. From a flow governing equations perspective, the viscous effects will be important where the second

derivative of the velocity $u(x,y)$ is significant. The question then becomes is how one would describe the location of this viscous sublayer. In a recent set of papers Weyburne [10,11] introduced a boundary layer description method based on the observation that the second derivative of the laminar velocity profile over a plate had a Gaussian-like appearance as illustrated in Fig. 1 ($_1$ will be defined shortly). The mathematical description of the viscous boundary layer region therefore borrows from probability density function (PDF) methodology and uses central moments of the second derivative-based kernel to describe the location and shape of the second derivative profile. Since the second derivative of the velocity is directly related to the viscous term in the momentum balance equation, we have termed this the "viscous" boundary layer description.

For wall-bounded 2-D flows, the viscous *n*th central moment $_n$ is

$$_n \equiv \int_0^h dy\,(y - \;_1)^n \frac{d^2\{-\;_1 u(x,y)/u_e\}}{dy^2}, \tag{2}$$

where $y=h$ is deep into the free stream, u_e is the free stream velocity at the boundary layer edge, and where the first moment about the origin, $_1$, is part of the normalizing parameter $(-\;_1/u_e)$ obtained as the requirement that $_0$ have a value of unity. The derivative in Eq. 2 is written in this way to emphasize the probability-density-function-like behavior.

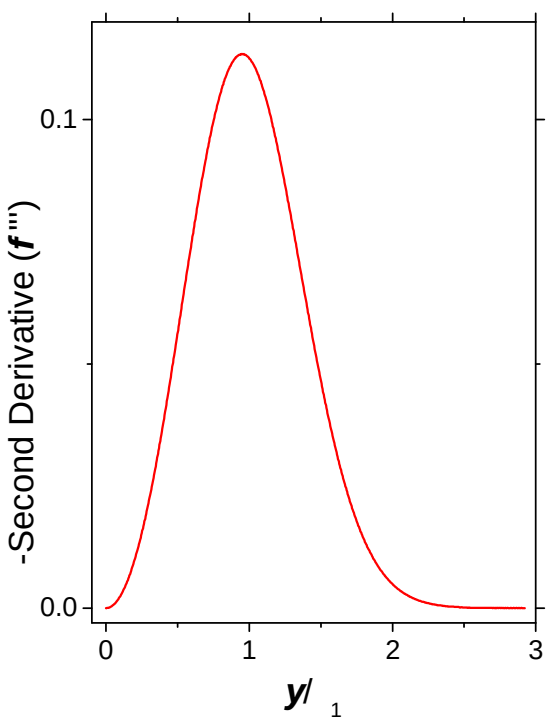

Figure 1: Second derivative of the velocity of the Blasius [12] solution for laminar flow.

Borrowing from probability density function (PDF) language, the first moment about the origin, $_1$ is called the "mean" location of the viscous sublayer. The mean location is therefore the center of action for the viscous sublayer for boundary layer flows. It easy to show that $_1$ for the Blasius laminar flow case is given by $_1 = \sqrt{x/u_e}\,/\,0.33206$ [10]. For the general case, the value of $_1$ is found by performing the integration of $_0$ so that

$$_1 = \frac{u_e}{\left.\dfrac{du(x,y)}{dy}\right|_{y=0}} = \frac{u_e}{\;_w}, \tag{3}$$

where $_w$ is the wall shear stress, is the kinematic viscosity, and is the density. In terms of the skin friction coefficient c_f, or the friction velocity u , this becomes

$$_1 = \frac{2}{u_e c_f} = \frac{u_e}{u^2} \quad . \tag{4}$$

Looking at Eq. 3, it now becomes clear that a change in the wall shear stress will have a direct effect on the mean location of the second derivative profile, and therefore on the velocity profile itself. It is evident that the center of action of the viscous sublayer, given by the mean location $_1$, is inversely proportional to $_w$. Therefore, a fluctuation of the wall shear stress means that the viscous sublayer is also undergoing a fluctuation away from or toward the wall depending on the instantaneous wall shear stress value.

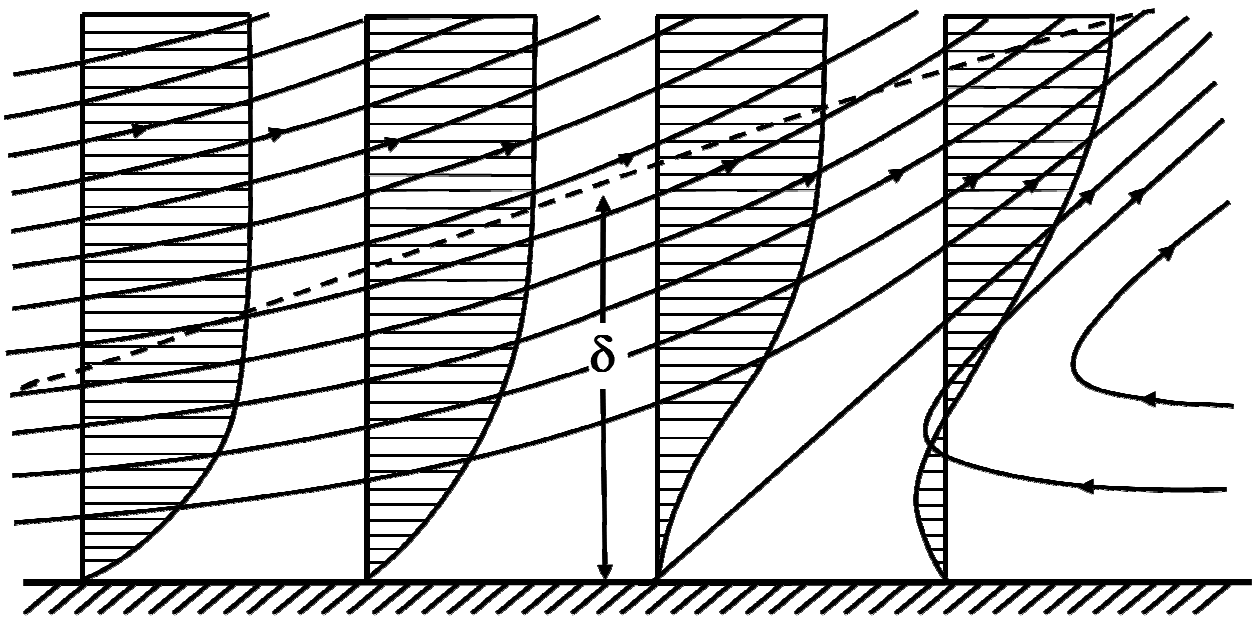

Figure 2: Diagrammatic depiction of flow along a wall undergoing separation.

The use of Eq. 3 means that the shear stress fluctuations have a direct quantifiable effect on the location of the viscous sublayer. Due to the importance of this point, we feel it is instructive to present a visual model to re-enforce this observation. In Fig. 2 we depict a simple schematic of a fluid flowing along a wall that is undergoing separation. The velocity gradients at the wall are going from positive to negative as one moves along the wall from left to right. If the velocity profiles are replotted in plus units, then they would all look similar according to the Law of the Wall (at least up to the point of separation). However, in actual dimensioned units these profiles are spread over a larger and larger boundary layer thickness . Hence the second derivative profiles, which would look something like Fig. 1, are becoming broadened which means that the mean location must be shifting away from the wall as one moves from left to right. Now imagine a turbulent boundary layer in which at any point on the wall the shear stress is going from almost zero (separation point) to a value many times larger than the average measured wall shear stress value. The same thing will happen in this case, the viscous sublayer will move closer to or further away from the wall depending on the instantaneous wall shear stress value. This then is the first important point to be made: for a wall-bounded turbulent boundary layer undergoing rapid time-varying changes in the wall shear stress, there must be an accompanying change in the spatial location of the viscous sublayer.

3. The Log Law Revealed

The next step is to tie these rapid changes of the viscous layer to the Log Law region. This is not a straightforward task as was discussed in the Introduction. Conventional thinking is that the viscous sublayer only extends from the wall to about $y^+ \cong 30$ into the fluid whereas the Log Layer only just starts where the viscous sublayer leaves off [6]. Conventional thinking may in fact be correct in terms of contributions to the momentum equation. However, in terms of contributions to the "tail" of the viscous sublayer, we can show that the Log Law region is an integral part of the tail region of the second derivative profile. In Figs. 3-6 we plot a number of experimental turbulent boundary layer velocity profile datasets that show Log-Law-type behavior (additional examples are given in the Appendix 1). In Figs. 3a to 6a we plot the datasets using the classic Log Law "plus" unit scaling. In Figs. 3b to 6b the velocity profile datasets are twice differentiated to yield the second derivative profile plots. The differentiation was done using the simple 2-point numerical differentiation formula. It is known that numerical differentiation is unstable in the presence of noise so it is necessary to use high quality datasets like those in Figs. 3-6 in order to see Log Law behavior in the second derivative profiles. Note that some of plots look discontinuous due to the fact that in some cases the numerical second derivatives generated negative values which do not plot on a Log scale. We made no attempt to fix these values and plotted the data by simply leaving out the negative values. In spite of the noisy look to some of these plots, it is apparent that in the regions in which the velocity profile is following the Log Law profile, the second derivative profile plots also follow the Log Law in these same regions. The plots of the experimental data make it clear that the viscous sublayer extends all the way into the Log Law region.

This then is the basis of the new theory of the origin of the Log Law region. Time-varying wall fluctuations of the wall shear stress cause the viscous sublayer to move toward-away from the wall depending on the value of the instantaneous wall shear stress. These fluctuations extend down into the Log Law region. These insights are well supported by experimental results. What is unknown at this point is the actual shape of the instantaneous second derivative profile. It is not experimentally possible to measure the instantaneous velocity profile in a wind tunnel at the present time. Alternatively one could use DNS computer results. While this is an option we are presently exploring, it was not deemed possible from a time perspective for inclusion in this manuscript. We therefore theorize as to the shape of the tail of the instantaneous second derivative profile.

4. Instantaneous Second Derivative Profile Model

The one unknown at this point in time is the actual shape of the instantaneous second derivative profile. In lieu of the actual profile, we make the following conjecture: The tail of the instantaneous second derivative profile has the same shape as the laminar-like second derivative profile tail. What we actually expect to see is a distorted laminar-like second derivative profile tail. However, for illustrative purposes we will assume the entire shape is laminar-like. What we will attempt to do in this section is show how the Log Law behavior is created by time-averaging a whole range of laminar-like peaks whose wall shear-stress values range from almost zero to a value many times larger than the measured average value as observed experimentally. It would then be possible to average this range of second derivative profiles if one had, or could measure, the frequency of occurrence of the wall shear stress values (as done by Obi, et. al. [8] for example).

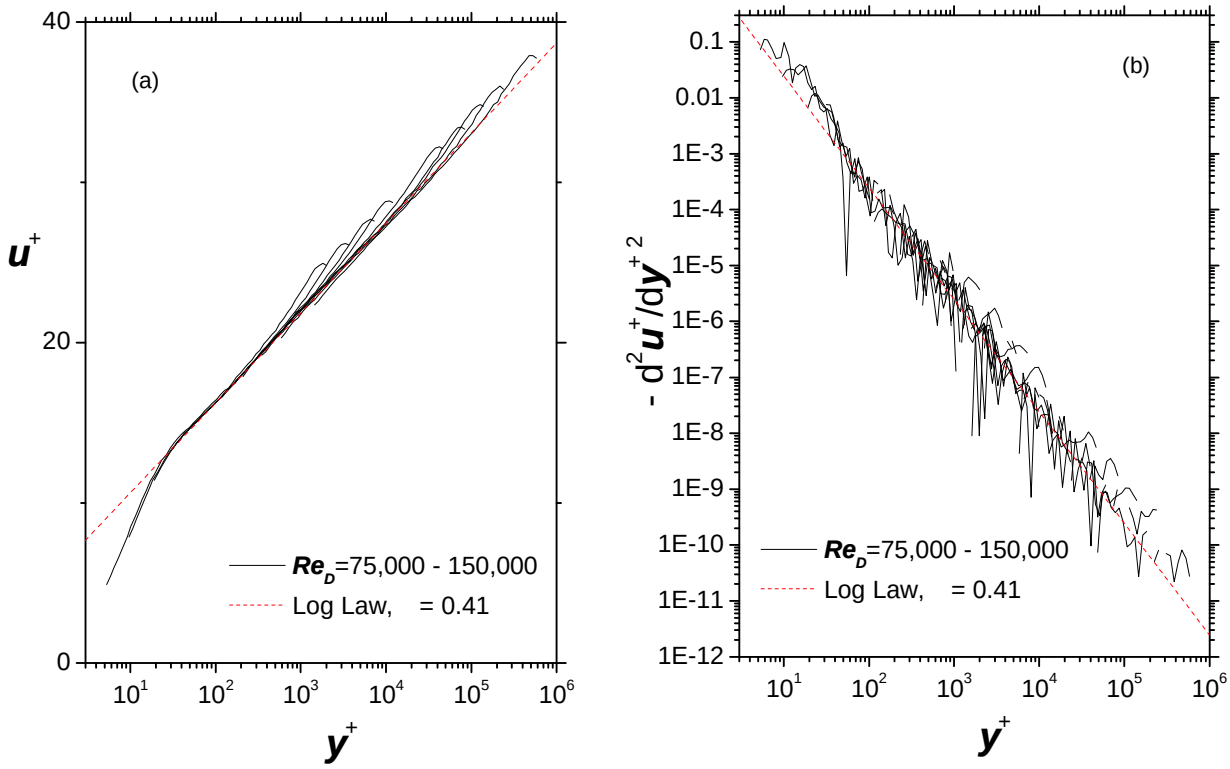

Figure 3: The solid lines are the McKeon, *et. al*. [13] Super Pipe profiles plotted in plus units. The dashed line is the Log Law line.

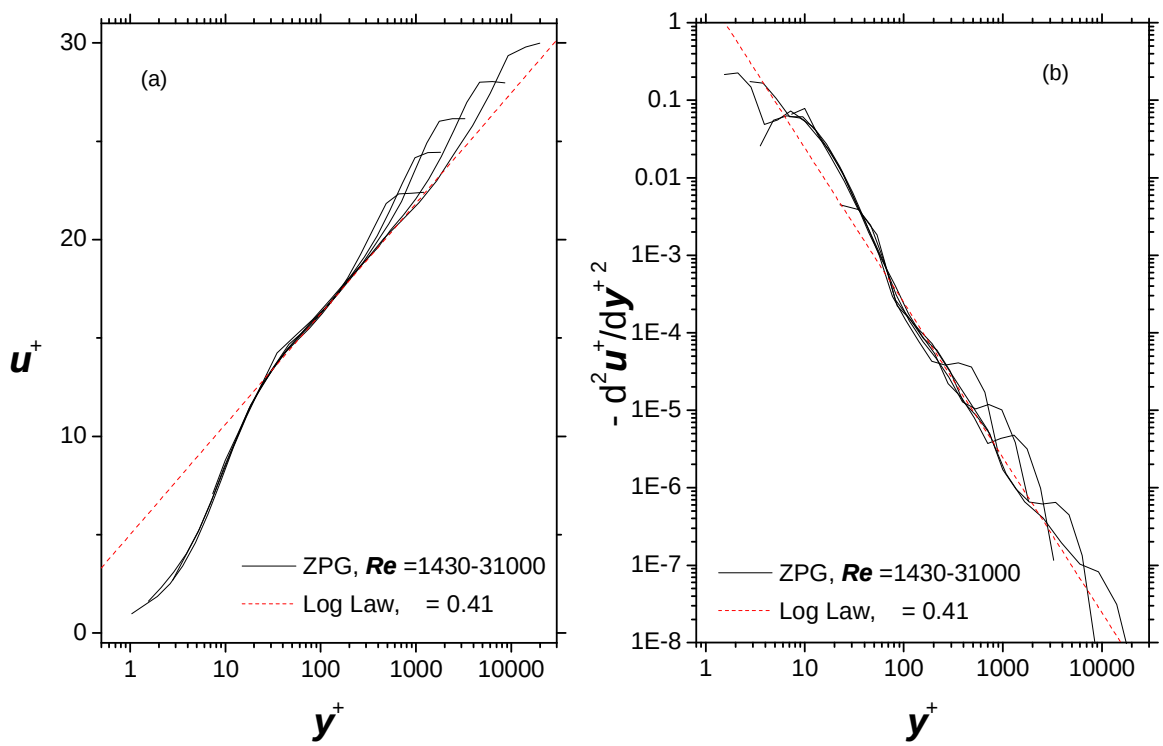

Figure 4. The solid lines are the DeGraaff and Eaton [14] ZPG profiles plotted in plus units. The dashed line is the Log Law line.

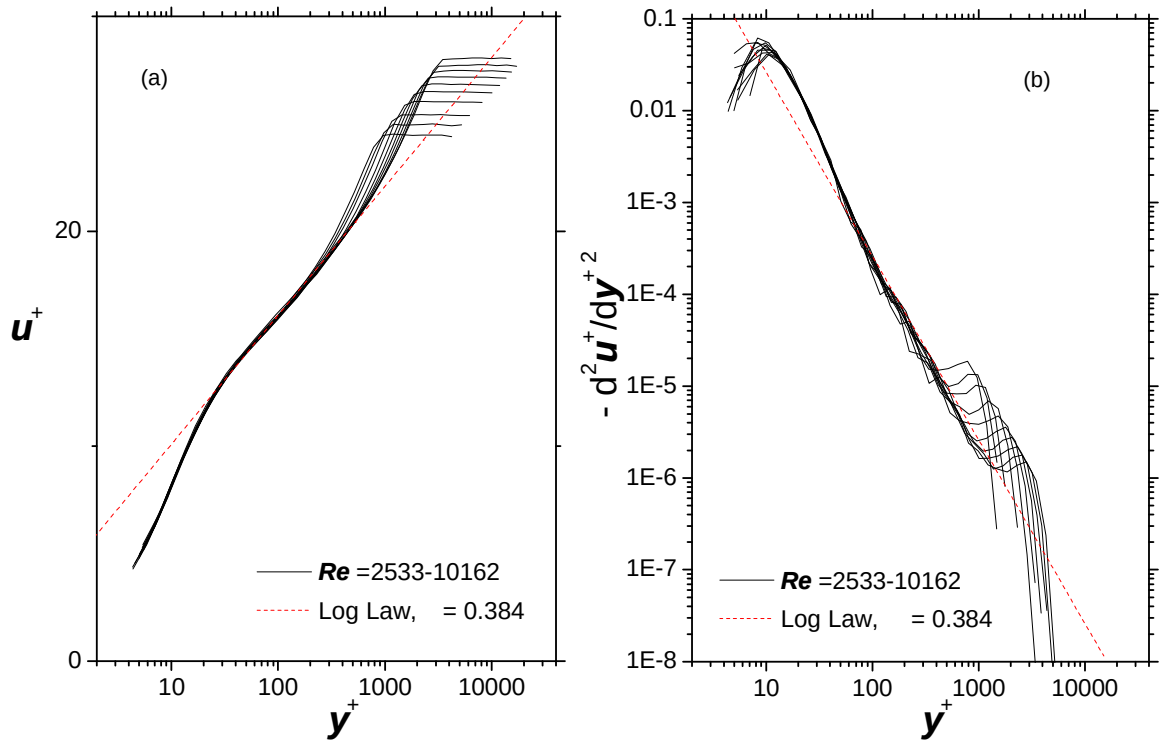

Figure 5: The solid lines are the Österlund [15] SW981129 profiles plotted in plus units. The dashed line is the Log Law line.

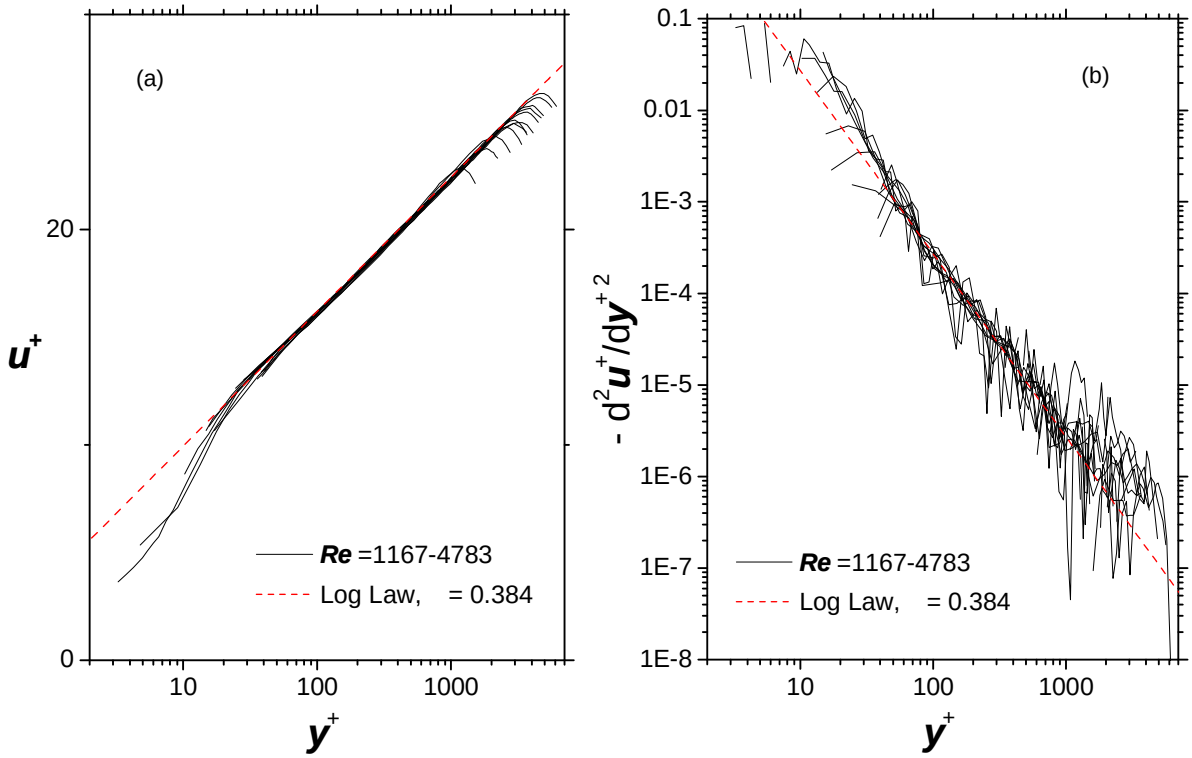

Figure 6: Black lines are the Zanoun and Durst [16] channel flow profiles plotted in plus units. The dashed line is the Log Law line.

For this exercise we will use the DNS data of Wu and Moin [9]. The Wu and Moin simulation is of a nominally-zero-pressure-gradient (ZPG) incompressible boundary layer over a smooth flat plate. The available datasets consist of a number of spatially developing profiles including laminar-like velocity profiles, transitional-like velocity profiles, and turbulent-like velocity profiles. In Fig. 7 we plot two profiles obtained by twice differentiating two of the velocity profiles. The solid black line is the reported velocity profile closest to the front of the plate and corresponds to a laminar-like profile. This was verified by calculating $_1 / \ _1$, where $_1$ is the displacement thickness. This value was found to be within 2% of the Blasius laminar value [11]. The dashed blue line in Fig. 7 is the farthest reported profile from the front of the plate and is considered turbulent-like. The red dotted line in Fig. 7 is the Log Law line added for reference. It is evident that the blue turbulent-like line is not following the Log Law very well, probably due to the fact that the Reynolds number for this dataset is rather low [15]. Never-the-less, we can see that it has the right trend. Notice how fast the tail of the laminar-like profile is decaying compared to the turbulent-like tail.

The fundamental question to be answered herein is how one goes from the laminar-like profile (solid black line) to the turbulent-like profile (dashed blue line). The first point was made in Section 2, namely that it is known that at a given point on the wall, the turbulent boundary layer is undergoing rapid changes in the wall shear stress [7-9]. These rapid changes in the wall shear stress result in an accompanying change in the mean location of the viscous layer of the boundary layer which we have just shown extends into the Log Law region.

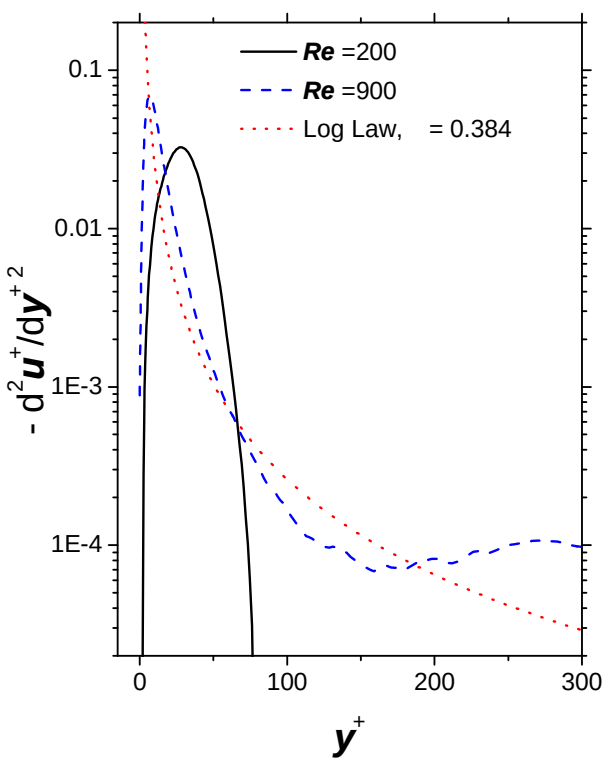

Figure 7: Second derivative profiles of Wu and Moin [9] plotted in plus units.

To see how we would go from a curve that is declining exponentially (Gaussian) away from the wall to the one-over-distance-from-the-wall-squared Log Law behavior, consider that Wu and Moin indicate that the skin friction coefficient c_f at any point on the plate varies from almost zero to a peak value that is four to five times larger than the mean [9]. Now consider Figure 8. In this plot, the solid black line is calculated by taking the laminar-flow profile shown in Fig. 7 and rescaling the plus unit values. The rescaling takes place by changing the friction velocity u from the laminar flow value to a friction velocity value that corresponds to a c_f value that is five times larger than the turbulent profile value (the profile at Re =900 in Fig. 8). It is easily shown using Eq. 4 that the mean location in plus units is inversely proportional to the friction velocity u . Hence a larger friction velocity will mean that the second derivative

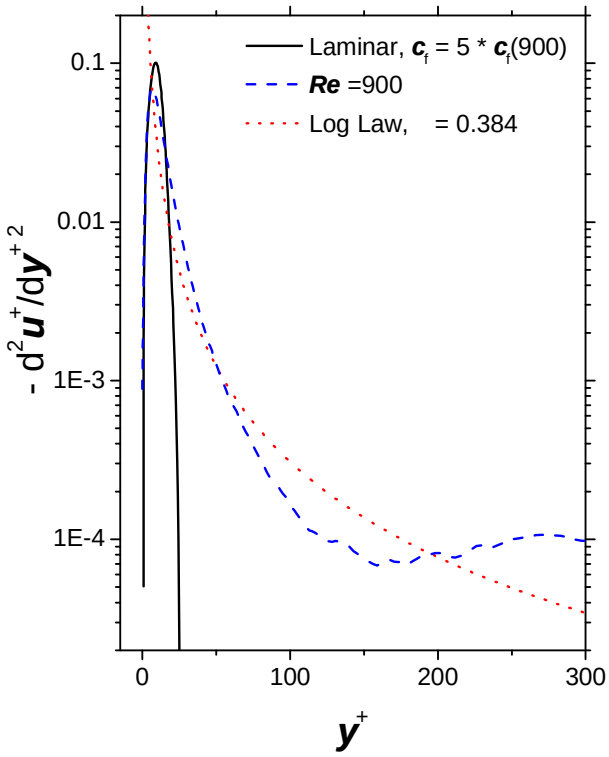

Figure 8: Same as Fig. 7 but with modified laminar profile such that c_f is 5 times lager.

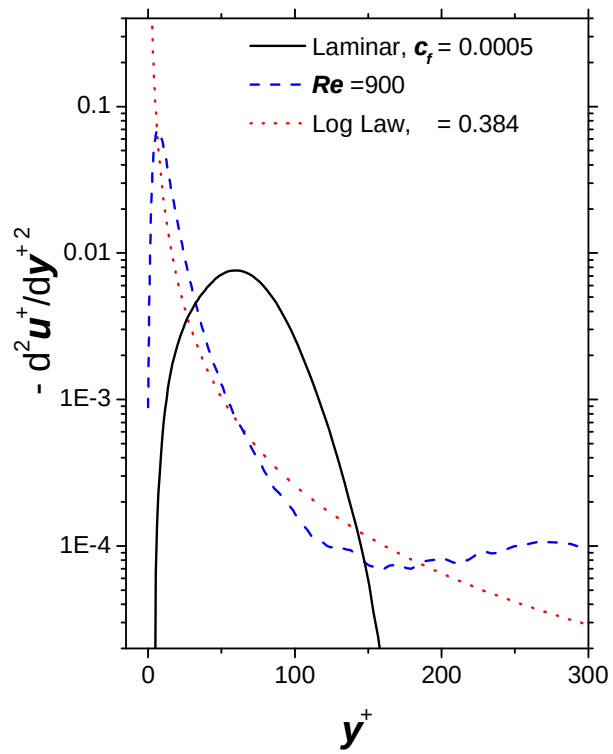

Figure 9: Same as Fig. 7 but with modified laminar profile such that c_f =0.0005.

profile will shift toward the wall as shown in Fig. 8. On the other hand, the plus scaled second derivative scales as u so that a larger friction velocity means that the amplitude of the second derivative profile will increase as shown in Fig. 8 (see Appendix 2).

The next step is to see what happens when the skin friction coefficient value goes in the other direction and approaches zero. From Wu and Moin's Fig. 8, it appears the smallest skin friction coefficient they measured was $c_f \cong 0.0005$ [9]. Consider what would happen if we rescale the laminar-like profile from Fig. 7 with a friction velocity value that corresponds to a c_f =0.0005 value. This is shown in Fig. 9. In this plot, the black line is again calculated by taking the laminar-flow profile shown in Fig. 7 and rescaling the plus unit values. Obviously the trends on the location and amplitude of the second derivative profile is opposite to what we saw when c_f became larger rather than smaller than the average value. In this case the peak moves away from the wall and the peak amplitude becomes smaller.

The results shown in Figures 8 and 9 are approximate instantaneous snap shots of what might be happening to a turbulent second derivative profile during the extreme swings in the skin friction coefficient. Wu and Moin indicate that the skin friction coefficient is rapidly fluctuating between these extreme values. Thus, what we would expect is a whole spectrum of these laminar-like spikes with mean values/amplitudes varying from Fig. 8-like to Fig. 9-like. Given the PDF of the frequency of occurrence, as shown for example in Fig. 10, one could average all the spikes to presumably obtain the turbulent blue line in Figs. 7-9. This then is a simplified model of the origin of Log Law behavior seen in wall-bounded turbulent boundary layers.

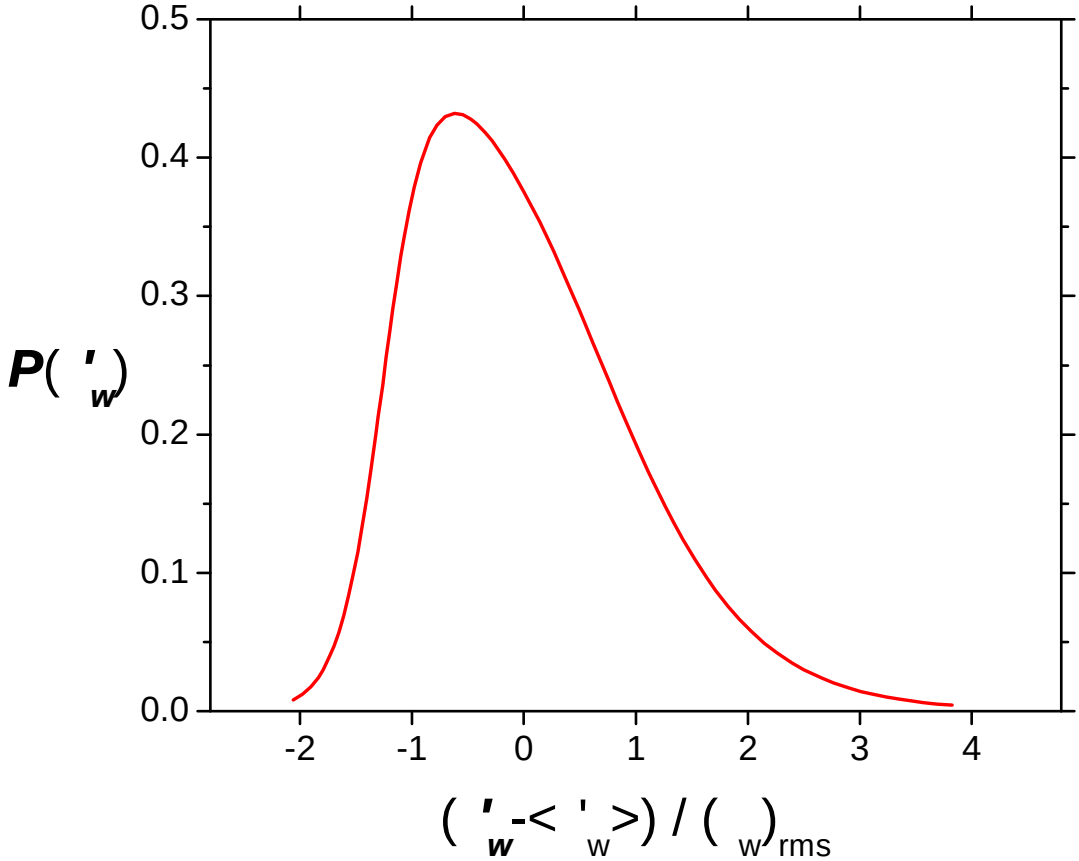

Figure 10: A recreation of Figure 7 from Obi, *et. al*. [8] showing a measured PDF of the instantaneous wall shear stress at a point on the wall.

5. Discussion

At first glance it may be perplexing as to why we choose to use the second derivative velocity profile to discuss the origin of the Log Law region in the velocity profile of a turbulent boundary layer. It is in fact possible to make many of these same arguments using just the velocity profile. The advantage of using the second derivative profile is twofold. First, the position of the mean location of the second derivative profile can be directly tied to the wall shear stress value through Eq. 3. This provides an easy path to visualize the effect of fluctuations of the wall shear stress that occur at the wall of a turbulent boundary layer. The second advantage of using the second derivative profiles is that the shape of the second derivative profiles provided a clue as to the origin of the Log Law region. When one looks at the second derivative of a laminar profile and a turbulent profile, Fig. 7 for example, it is apparent that the major difference is in the tail region of the profile. It was trying to understand how the tail could become stretched out that led to the theory presented herein.

The realization that the Log Law behavior is based on rapid fluctuations of the velocity profile explains why previous theoretical studies based on time-averaged governing equations have not been able to explain the physical origin of the Log Law behavior. It is in fact the time-averaging process of the instantaneous changes in the position of the viscous layer that results in the

logarithmic behavior. What is exciting about the new theory is that it opens up a whole new way to experimentally attack some of the outstanding questions of wall-bounded turbulent boundary layers. For example, it should be possible to say something more definitive about the empirical constant and whether it truly is universal by looking at the evolution of the instantaneous second derivative profile wall shear stress frequency of occurrence PDF spectrum as the Reynolds number increases for the different type of wall-bounded flows. It should also be possible to say something about the physical extent of the Log Law and why the Log Law extends so much farther into the fluid for pipe flow as opposed to flow over a plate.

The key to the new theory for the origin of the Log Law region are two important insights. The first key insight is related to the fact that experimental work [7-9] makes it clear that the wall shear stress $_w$, or equivalently the skin friction coefficient c_f, undergo very large fluctuations at any point on the wall in the turbulent flow region. This leads to the most important insight provided herein and that is that these changes in the wall shear stress induce large, quantifiable fluctuations in the location of the viscous sublayer in the boundary layer. This is because the center of action in the viscous region, given by the mean location $_1$, is inversely proportional to $_w$ according to Eq. 3. Time-varying fluctuations in $_w$ will therefore induce spatial fluctuations in $_1$ and the viscous sublayer in total. Note that $_1$ tracks the center location of the viscous region. The width and amplitude of the peak are also varying with $_w$. For the work herein we made the assumption that the width and amplitude of the instantaneous turbulent second derivative profile behaves similar to the laminar flow second derivative profile (Appendix 2). From the few turbulent datasets that we have checked, the width assumption seems to be a reasonable approximation. In any case, the basis of the new theory on the origin of the Log Law region is that if one spatially averages these instantaneous viscous shear layer changes, one will find that the normal instantaneous second derivative decay behavior is stretched out into a one-over-distance-from-the-wall-squared behavior associated with the Log Law for turbulent layers.

The second important insight provided herein is these fluctuations extend into the Log Law region. This is somewhat contrary to conventional thinking that has assumed that the viscous shear is negligible in the Log Law region of the boundary layer. Conventional thinking may in fact be correct in terms of contributions to the momentum equation. However, in terms of contributions to the "tail" of the viscous sublayer, we showed that the Log Law region is an integral part of the tail region of the second derivative profile. Looking at Figs. 3b-6b as well as the figures in the Appendix 1, one sees that the second derivative profiles tracks the Log Law rather well. Therefore there is ample experimental support to say that the fluctuations of the viscous sublayer show up all the way into the Log Law region.

The major unknown in the new theory is the shape of the instantaneous second derivative profile. We speculated that the tail of the turbulent instantaneous second derivative profile has the Laminar-like Gaussian tail as one moves further away from the wall. What we actually expect to see is a distorted instantaneous second derivative profile due to the turbulent motion. From a physical perspective, there is a good reason to assume that the second derivative profile of turbulent flow should decay in the same Gaussian-like decay behavior of laminar flow (see Fig. 1) into the fluid. The timescales for the turbulent motion are many orders of magnitude longer than the time scales normally associated with the molecular diffusion time scales of the viscous forces. Hence the main factor affecting the shape of the velocity profile (besides fluid properties) will be the instantaneous wall shear stress value and the free stream velocity. For

comparable values, we would expect that the laminar second derivative profile and the instantaneous turbulent second derivative profile should decay similarly. The mitigating factor is the extent that the turbulent motion itself induces viscous forces sufficient to change the instantaneous second derivative profiles. This will be dependent on the magnitude of the second derivative of the instantaneous u and v velocities compared to the average second derivative $u(x, y)$ velocity values. In general, this ratio is probably small but in fact the changes to the tail region are small compared to the peak of the second derivative profile. At this point in time it is difficult to quantify these contributions. From examination of Fig. 9 which shows the farthest from the wall stretched out laminar-like curve, it is obvious that the blue turbulent-like tail region is getting contributions at $y^+ > 200$ that would be hard to explain using the theory discussed above. However, these contributions may be of the "wake" type shown in Figs 3b-6b. Notice that the second derivative "wake" type structures do not display similarity using the plus scaling. It is therefore possible that the theory described above explains the similarity aspects of the plus scaling in the inner region and the turbulent-induced motion explains the wake portion of the second derivative profiles. It may be possible to use DNS experiments as a way of teasing out the extent that these instantaneous velocity changes are affecting the tail region. This is an option we are presently exploring, but it was not deemed possible from a time perspective for inclusion in this manuscript. We therefore introduced the simplified model assuming the Gaussian-like tail to show how the overall process might work. In this simplified model we directly assumed that the instantaneous second derivative profiles retained the same basic shape as the laminar-like profile. With this assumption in place we showed how wall shear stress changes would produce a spread-out tail consistent with the time-averaged turbulent second derivative profile.

The theory on the origin of the Log Law behavior presented herein explains how the instantaneous viscous shear layer changes from the (possible) Gaussian-like decay of the instantaneous turbulent velocity profile to the stretched out one-over-distance-from-the-wall-squared behavior of Log Law layer. However, it is apparent from looking at experimental plots both herein and elsewhere that the Prandtl length and velocity scaling parameters works not only in the Log Law region but also in the inner near wall region. In fact, it is now apparent from Figs. 3b-6b that the Log Law region is part of the viscous inner layer region, not some overlap region as is conventionally assumed. It is remarkable that the turbulent boundary layer literature has been almost totally silent on this issue of inner layer similarity. This may be explained at least in part by the fact that in the Log Law region the velocity profile is following an analytical functional form. One had the hope that a boundary layer theory could be found in which an analytical function would result after sufficient manipulations of the governing equations (which of course is the eddy viscosity/mixing length model). For the inner region one does not have this theoretical route. One only has empirical data. That is until now. It is clear that the same time-averaging mechanism of $_w$ also applies to the inner region similarity. The mechanism of similarity must is some fashion be related to the frequency PDF of the instantaneous $_w$ values which in turn must scale with the average $_w$ value. This tie-in of the average $_w$ value is needed to explain the success of the Prandtl "plus" scaling.

This linking of the inner region and the Log Law region was explained in part by a recent paper by Weyburne [17]. In this paper semi-empirical arguments were made to show that the Prandtl length scale $/u$ (actually ~15 $/u$), rather than $_1$, is a better tracker of the mean

location of the second derivative profile for the turbulent boundary layer. This means that $/u$ tracks the viscous contributions for the wall-bounded turbulent flow case. The viscous contributions in turn control the flow behavior in the inner region. Therefore, even though the work herein was targeted at describing the origin of the Log Law behavior in turbulent flows, it is apparent that it also describes, in part, the origin of similarity of the velocity profiles in the inner region using the Prandtl length and velocity scales.

6. Conclusion

A theory for the physical origins of the Log Law behavior of a wall-bounded turbulent boundary layer has been outlined. The keys to the new theory are twofold. First, the turbulent boundary layer fluid undergoes rapid, quantifiable changes in the wall shear stress at any point on the surface which give rise to rapid changes in the location of the viscous sublayer of the velocity boundary layer. The second key to the new theory is that experimental results were used to show that the viscous shear, which is directly proportional to the second derivative of the velocity profile, extends all the way into the Log Law region of the boundary layer. When this viscous layer is time averaged, one finds that the (possible) Gaussian-like decay of the viscous shear is stretched out into a one-over-distance-from-the-wall-squared behavior. The classic logarithmic profile behavior of the Log Law is obtained when this viscous shear profile is twice integrated to obtain the velocity profile perpendicular to the wall.

References

[1] O. Reynolds, “An experimental investigation of the circumstances which determine whether the motion of water in parallel channels shall be direct or sinuous, and of the law of resistance in parallel channels,” Phil. Trans. R. Soc., **174**, 935 (1883).

[2] T. von Kármán, "Mechanische Ähnlichkeit und Turbulenz", Nachr. Ges. Wiss. Goettingen, Math.-Phys. Kl., **5**, 58 (1930) (also as: “Mechanical Similitude and Turbulence”, Tech. Mem. NACA, no. 611, 1931).

[3] L. Prandtl, “ Bemerkungen zur Theorie der freien Turbulenz,” ZAMM, **22**, 241(1942).

[4] C. Millikan, *Proceedings Fifth Int. Conference Appl. Mech.*, (Wiley, New York, 1938).

[5] M. Oberlack, “A unified approach for symmetries in plane parallel turbulent shear flows,” J. Fluid Mech., **427**, 299 (2001).

[6] W. K. George, “Is there a universal log law for turbulent wall-bounded flows?” Philos. Trans. R. Soc. London, Ser. A **365**, 789 (2007).

[7] S. Robinson, “Instantaneous Velocity Profile Measurements in a Turbulent Boundary Layer,” Chem. Eng. Comm., **43**, 347 (1986).

[8] S. Obi, K. Inoue, T. Furukawa, and S. Masuda, “Experimental study on the statistics of wall shear stress in turbulent channel flows,” Int. J. Heat and Fluid Flow, **17**, 187 (1996).

[9] X. Wu and P.Moin, “Direct numerical simulation of turbulence in a nominally zero-pressure-gradient flat-plate boundary layer,” J. Fluid Mech., **630**, 5 (2009).

[10] D. Weyburne, “A mathematical description of the fluid boundary layer,” Applied Mathematics and Computation, **175**, 1675 (2006). Also D. Weyburne, Erratum to “A mathematical description of the fluid boundary layer,” Applied Mathematics and Computation, **197**, 466(2008).

[11] D. Weyburne, “New Shape Parameters for the Laminar, Transitional, and Turbulent Velocity Profiles,” Air Force Technical Report, DTIC number AFRL-RY-HS-TR-2010-0016, 2010.

[12] H. Blasius, “Grenzschichten in Flüssigkeiten mit kleiner Reibung. Zeitschrift für Mathematik und Physik,” **56**, 1 (1908).

[13] B. McKeon, J. Li, W. Jiang, J. Morrison, and A. Smits, “Further observations on the mean velocity distribution in fully developed pipe flow,” J. Fluid Mech., **501**, 135 (2004).

[14] D. B. DeGraaff and J. K. Eaton, ‘‘Reynolds number scaling of the flat plate turbulent boundary layer,’’ J. Fluid Mech., **422**, 319 (2000).

[15] J. M. Österlund, “Experimental studies of zero pressure-gradient turbulent boundary layer.” PhD. Thesis, Kungl Tekniska Högskolan (Royal Institute of Technology), 1999.

[16] E. Zanoun and F. Durst, “Turbulent momentum transport and kinetic energy production in plane-channel flows”, Int. J. Heat and Mass Transfer, **52**, 4117 (2009).

[17] D. Weyburne, “Similarity Scaling for the Inner Region of the Turbulent Boundary Layer,” Air Force Technical Report, DTIC number AFRL-RY-HS-TR-2010-0012, 2010.

[18] M. Simens, J. Jimenéz, S. Hoyas, and Y. Mizuno, “A high-resolution code for turbulent boundary layers,” J. Computational Physics, **228**, 4218(2009).

[19] P. Schlatter, R. Örlü, Q. Li, G. Brethouwer, J. Fransson, A. Johansson, P. Alfredsson, and D. Henningson, “Turbulent boundary layers up to Re =2500 studied through simulation and experiment,” Phys. of Fluids, **21**, 051702(2009).

[20] G. Khujadze and M. Oberlack, “DNS and scaling laws from new symmetry groups of ZPG turbulent boundary layer flow,” Theoret. Comput. Fluid Dynamics, **18**, 391(2004).

[21] S. Hoyas and J. Jimenez, “Scaling of the velocity fluctuations in turbulent channels up to Re =2003,” Phys. of Fluids, **18**, 011702 (2006).

[22] P. E. Roach and D. H. Brierley, “The Influence of a Turbulent Free-Stream on Zero Pressure Gradient Transitional Boundary Layer Development including the T3A & T3B Test Case Conditions.” In *Numerical Simulation of Unsteady Flows and Transition to Turbulence*,

edited by O. Pirnneau, W. Rodi, I. Ryhming, A. Savill, and T. Truong (Cambridge University Press, New York, 1992), pp 319-347.

[23] W. Bauer, "The Development of the Turbulent Boundary Layer on Steep Slopes," Ph.D. Thesis, Iowa State University, 1951. Data from D. Coles and E. Hirst, eds., *Proceedings of Computation of Turbulent Boundary Layers, AFOSR–IFP–Stanford Conference*, Vol. 2, (Thermosciences Div., Dept. of Mechanical Engineering, Stanford Univ. Press, Stanford, CA, 1969).

[24] K. Wieghardt and W. Tillmann, "On the Turbulent Friction for Rising Pressure,' NACA TM 1314 (1951). Data from D. Coles and E. Hirst, eds., *Proceedings of Computation of Turbulent Boundary Layers, AFOSR–IFP–Stanford Conference*, Vol. 2, (Thermosciences Div., Dept. of Mechanical Engineering, Stanford Univ. Press, Stanford, CA, 1969).

Appendix 1

The importance of the viscous behavior is central to the new theory of the origin of the Log Law for wall bounded turbulent boundary layers. Therefore, in this Appendix we present some addition experimental evidence that shows that the second derivaive profiles are following Log-Law-like behavior in the same region as the velocity profile is following Log-Law-like behavior. In Figures A1a to A8a we plot the datasets using the classic Log Law plus unit scaling. In Figures A1b to A8b the velocity profile datasets were twice differentiated to yield the second derivative profile plots. Since the derivatives are performed numerically, we have found that only high quality, low noise datasets work. For certain older, noisier datasets, the second derivates are too scrambled to see the trend line. The list of figures appearing in the Appendix 1 are as follows:

Figure A1. The solid lines are the Simens, *et. al*. [18] DNS ZPG profiles plotted in plus units. The dashed line is Log Law line. 18

Figure A2. The solid lines are the Schlatter, *et. al*. [19] DNS ZPG profiles plotted in plus units. The dashed line is Log Law line. 18

Figure A3. The solid lines are the Khujadze and Oberlack [20] DNS ZPG profiles plotted in plus units. The dashed line is Log Law line. 19

Figure A4. The solid lines are the Hoyas and Jimenez [21] DNS channel profiles plotted in plus units. The dashed line is Log Law line. 19

Figure A5. The solid lines are some of the T3A Roach and Brierley [22] flat plate profiles plotted in plus units. The dashed line is Log Law line. 20

Figure A6. The solid lines are the Zanoun and Durst [16] pipe flow profiles plotted in plus units. The dashed line is the Log Law line. 20

Figure A7. The solid lines are the Bauer [23] spillway flow profiles plotted in plus units. The dashed line is the Log Law line. 21

Figure A8. The solid lines are the Wieghardt and Tillmann [24] flat plate flow profiles plotted in plus units. The dashed line is the Log Law line. 21

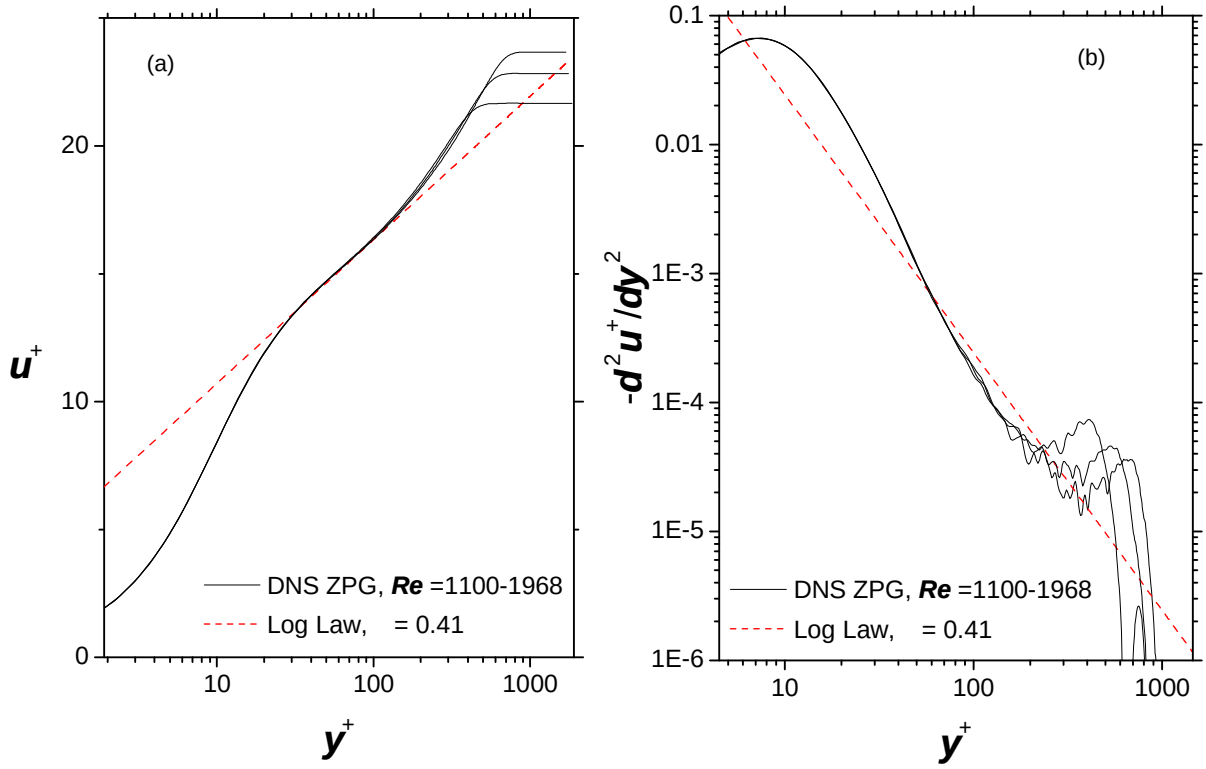

Figure A1: The solid lines are the Simens, *et. al*. [18] DNS ZPG profiles plotted in plus units. The dashed line is Log Law line.

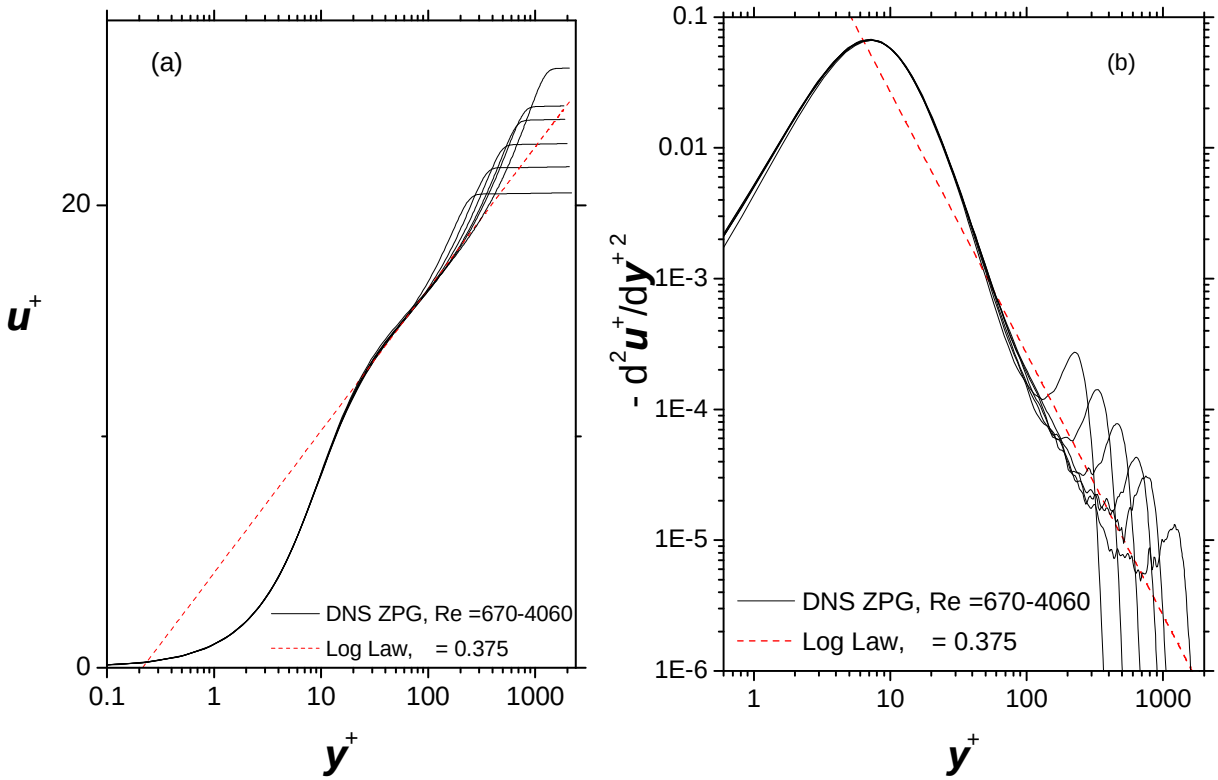

Figure A2: The solid lines are the Schlatter, *et. al*. [19] DNS ZPG profiles plotted in plus units. The dashed line is Log Law line.

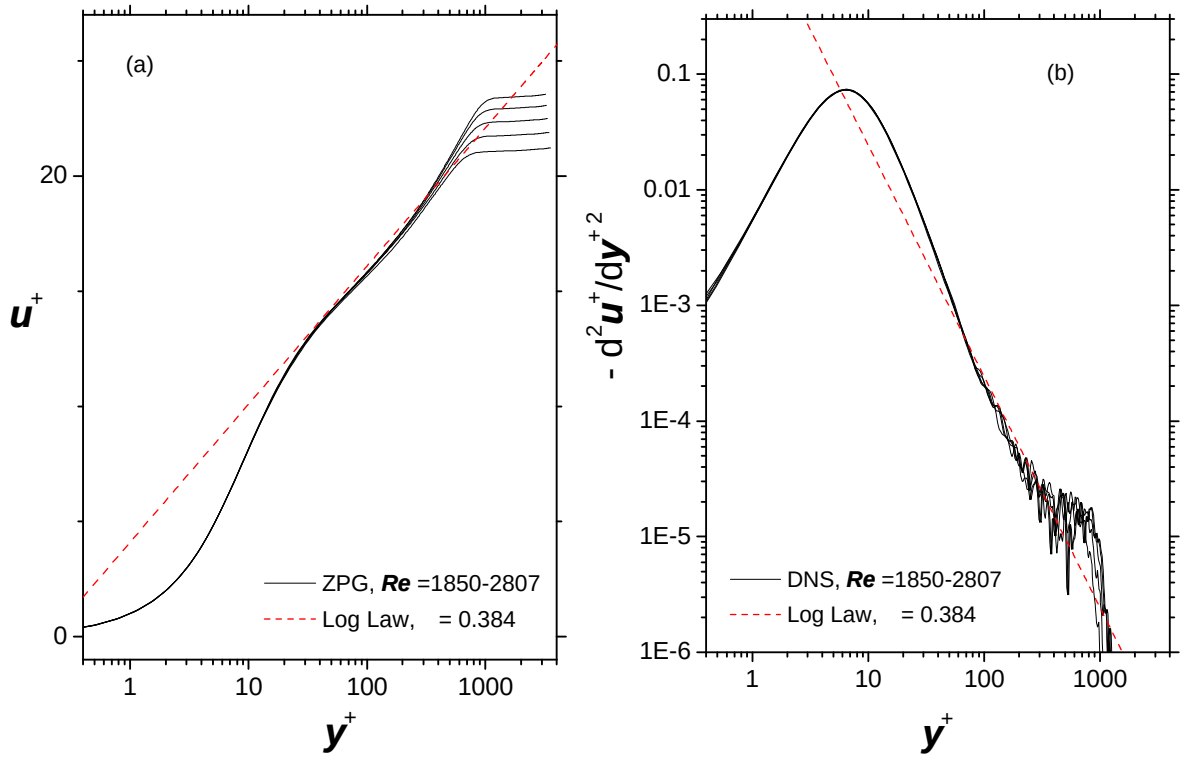

Figure A3: The solid lines is the Khujadze and Oberlack [20] DNS ZPG profiles plotted in plus units. The dashed line is the Log Law line.

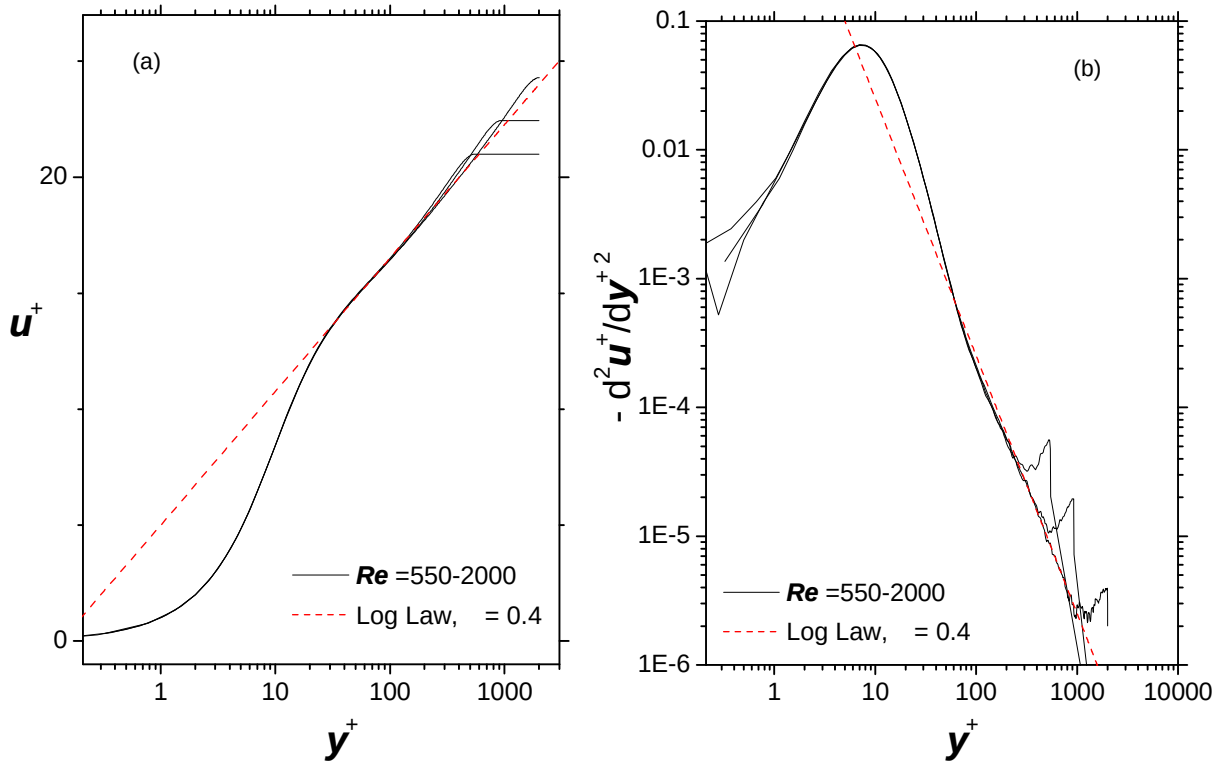

Figure A4: The solid lines is the Hoyas and Jimenez [21] DNS channel profiles plotted in plus units. The dashed line is the Log Law line.

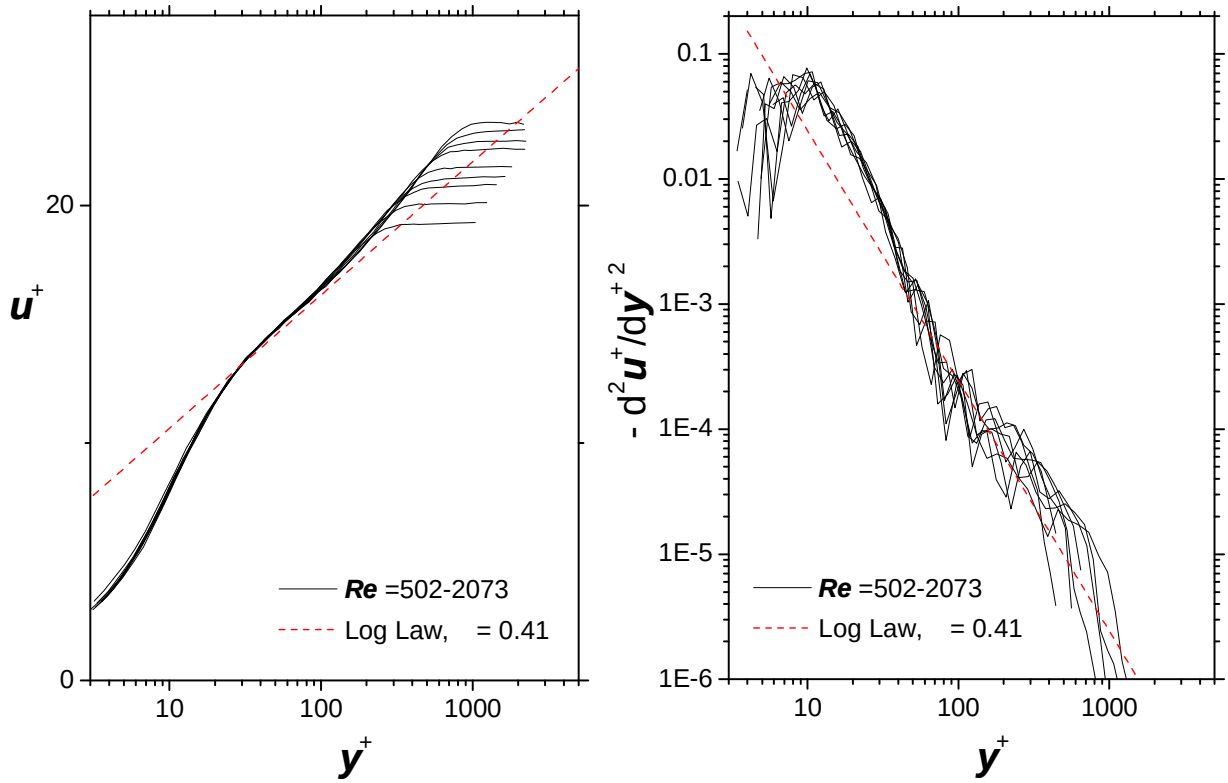

Figure A5: The solid lines are some of the T3A Roach and Brierley [22] profiles plotted in plus units. The dashed line is the Log Law line.

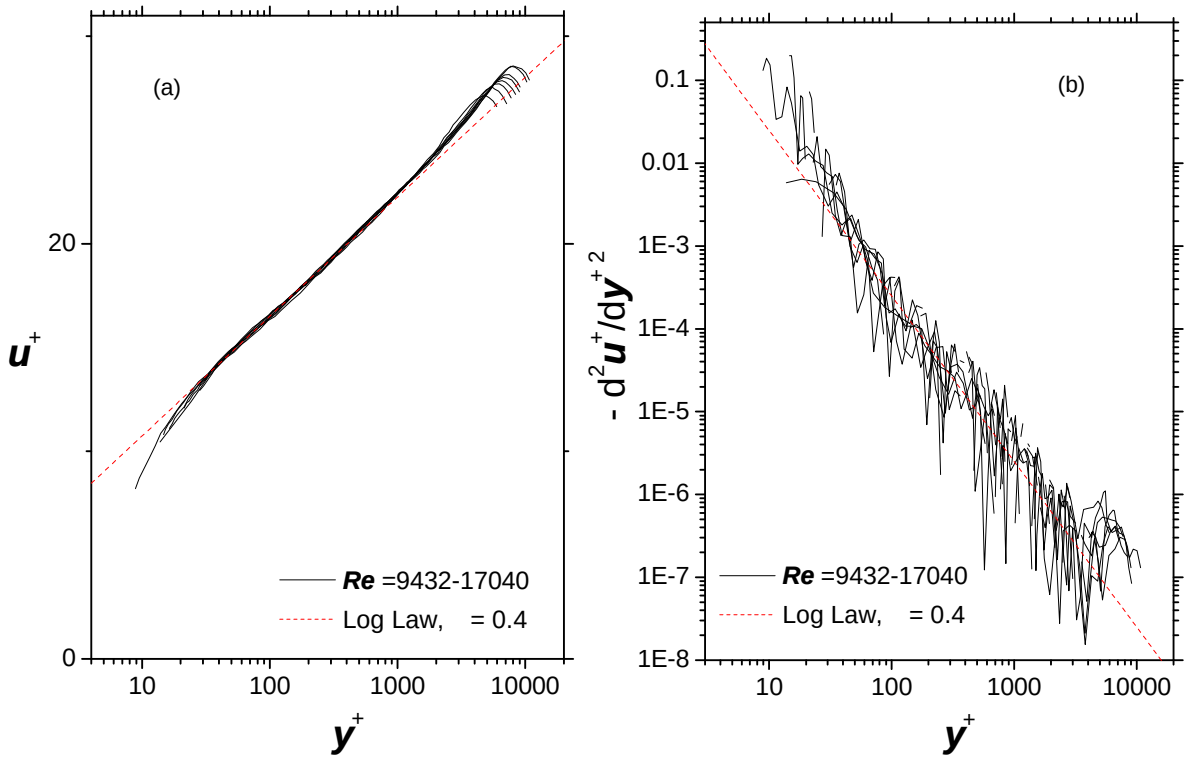

Figure A6: The solid lines are the Zanoun and Durst [16] pipe flow profiles plotted in plus units. The dashed line is the Log Law line.

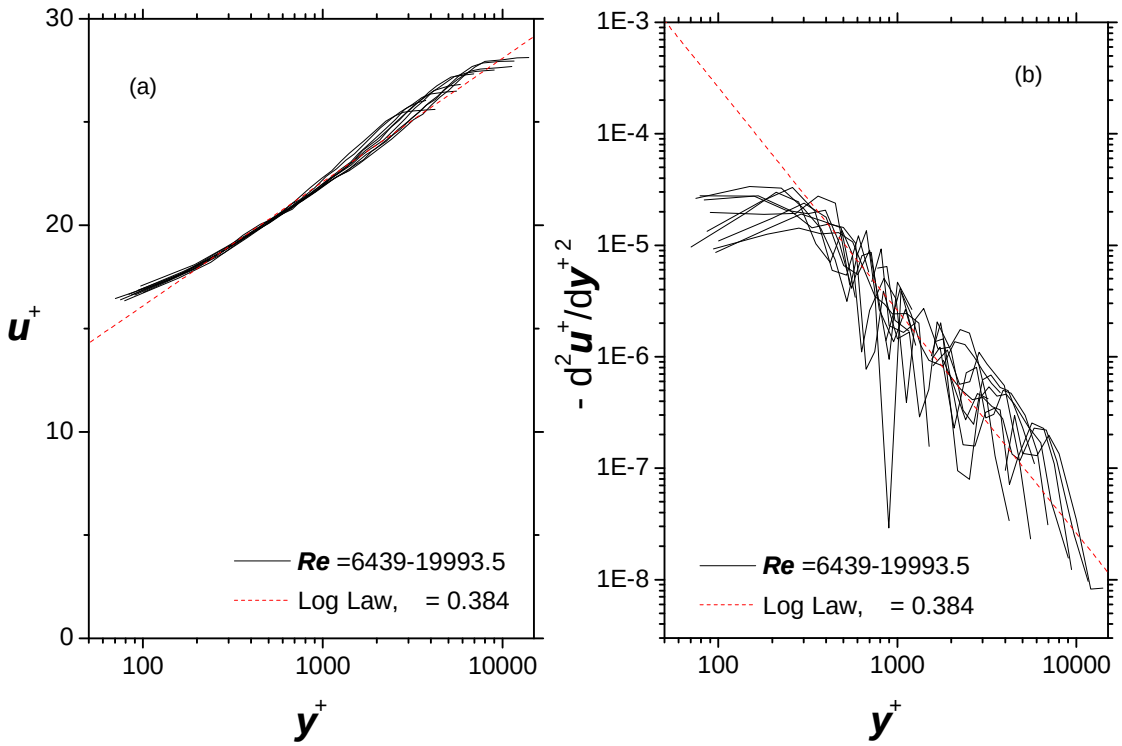

Figure A7: The solid lines are the Bauer [23] spillway flow profiles plotted in plus units. The dashed line is the Log Law line.

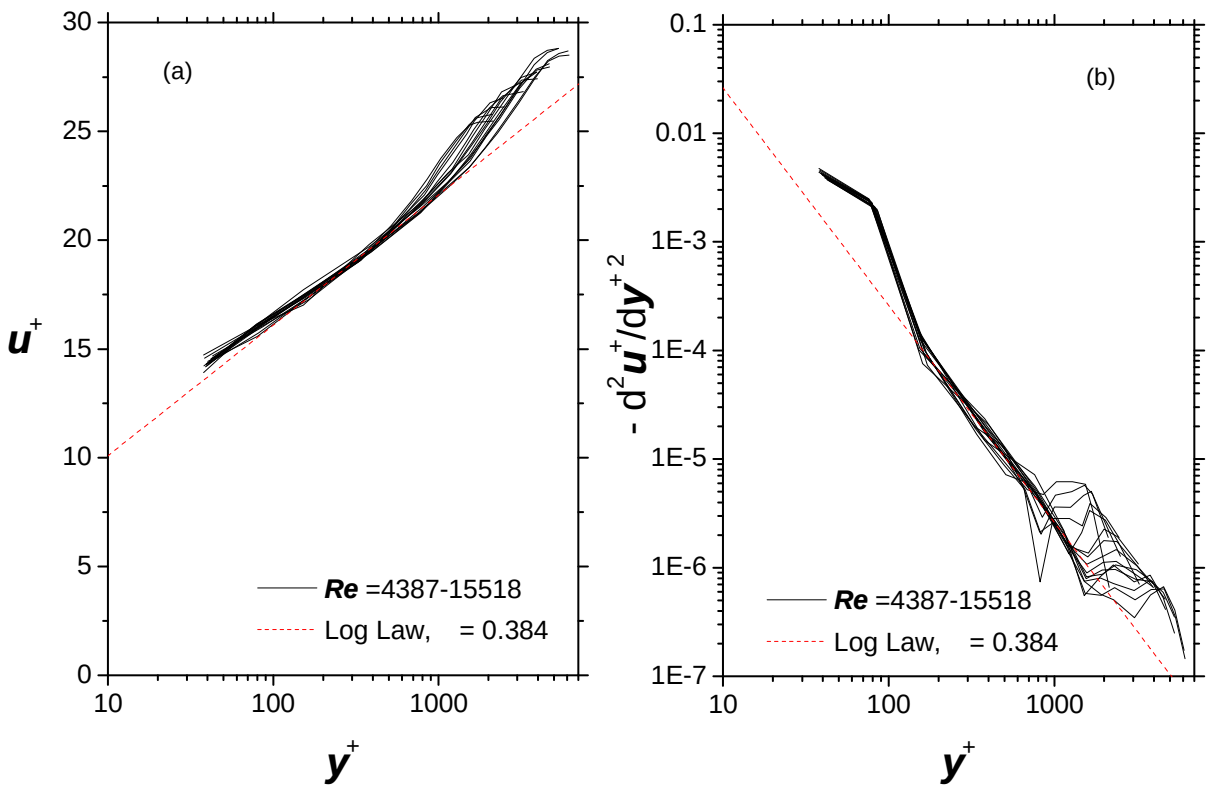

Figure A8: The solid lines are the Wieghardt and Tillmann [24] flat plate flow profiles plotted in plus units. The dashed line is the Log Law line.

Appendix 2

In Figs. 8 and 9 we need to rescale the laminar-like profile from the DNS data of Wu and Moin [9]. The rescaling of the mean location $_1$ is straightforward using Eq. 4. To do this rescaling we also need to know how the amplitude and width of the instantaneous second derivative of the velocity scales. At the present time, we do not know how the amplitude scales for the instantaneous case. We will therefore assume that the instantaneous turbulent second derivative amplitude scales in the same fashion as the laminar profile second derivative profile. For the laminar flow case, Weyburne [10] showed that the second derivative is well approximated by the Gaussian distribution function

$$\frac{d^2u(y)}{dy^2} \cong \frac{Cu_e}{_v\sqrt{2}} e^{-\frac{1}{2}\left(\frac{y-\ _1}{_v}\right)^2} \tag{A2.1}$$

where C is a constant, $_v$ is the viscous boundary width, and $_1$ is the mean location. The boundary conditions for this flow situation can be used to obtain the constant *C*. Weyburne [10] showed that in particular, $C = -2/(\ _1 s)$ where

$$s = 1 + ERF\left(\sqrt{2}\ _1/(2\ _v)\right) + \sqrt{2}\ _v EXP\left(-(\ _1/\ _v)^2/2\right)/(\ _1\sqrt{\ }) \quad . \tag{A2.2}$$

For laminar flow, and the work herein, the value of *s* is well approximated as *s*=2. This means

$$\frac{d^2u(y)}{dy^2} \cong \frac{-u_e}{_1\ _v\sqrt{2}} e^{-\frac{1}{2}\left(\frac{y-\ _1}{_v}\right)^2} \quad . \tag{A2.3}$$

The boundary layer width is given by $_v = \sqrt{2\ _1\ _1 - \ _1^2}$ where $_1$ is the displacement thickness [10]. For simplicity, we will assume that $_1$ is a simple multiple of $_1$ so that $_v \cong a\ _1$ where *a* is a constant. From an amplitude perspective, using Eq. 4 means

$$\frac{d^2u(y)}{dy^2} \cong \frac{-u^4}{a\ ^2u_e\sqrt{2}} e^{-\frac{1}{2}\left(\frac{y-\ _1}{_v}\right)^2} \quad . \tag{A2.4}$$

In plus units we have

$$\frac{d^2u^+}{dy^{+2}} \cong -\frac{u}{au_e\sqrt{2}} e^{-\frac{1}{2}\left(\frac{y^+-\ _1^+}{_v^+}\right)^2} \tag{A2.5}$$

which means the amplitude in plus units varies linearly with the friction velocity whereas $_1$ and $_v$ in plus units vary inversely with the friction velocity. These properties are used to rescale the laminar-like plot in Fig. 7 to the plots shown in Figs. 8 and 9.